Proceedings of the 1999 IEEE
International Conference on Robotics & Automation
Detroit, Michigan • May 1999

Position Control of a Compliant Mechanism Based Micromanipulator

Kevin Fite
Michael Goldfarb

Department of Mechanical Engineering
Vanderbilt University
Nashville, TN 37235

Abstract

This paper addresses the modeling and control of a compliant micromanipulator for use in such fields as microsurgery, telesurgery, and microassembly. The unique flexure-based manipulator utilizes revolute flexure joints in achieving well-behaved kinematic characteristics, without the backlash and stick-slip phenomena that would otherwise impede precision control. A mathematical model of the micromanipulator is formulated, and a controller for positioning of the manipulator is derived. The model and resulting controller are unlike typical manipulator models and controllers, since this manipulator is actually a controlled large range-of-motion structure with nonlinear structural dynamics. Following the development of the controller, computer simulations of the proposed controller on the manipulator are used to verify the positioning performance.

1 Introduction

Though considerable research has been directed toward the advancement of robotic manipulation on a conventional scale (i.e., millimeters to meters), relatively little work has been conducted on interactive robotic manipulation at a microscopic scale (i.e., microns to millimeters). Once developed, interactive micromanipulator technology will have application in many fields, including micromanufacturing, microsurgery, telesurgery, microbiology and pharmaceutical research. Many microscale parts, for example, have been fabricated utilizing photo lithographic and X-ray lithographic microfabrication techniques. Despite these advanced microfabrication techniques, fully functional multi-element microelectromechanical (MEMS) devices have not yet come to fruition, due in part to the inability to assemble the very small parts, and in particular to assemble in large quantities (i.e., mass produce). A micromanipulator would enable dexterous handling of micromanufactured parts, and thus enable assembly of functional MEMS devices. If utilized in a teleoperative sense, a macromanipulator master coupled to a micromanipulator slave could enable dexterous human-controlled telemanipulation of a microscopic environment. In this sense, the telemanipulation system would address human positioning limitations in the forward path and limited human force sensitivity in the backward path. Coupled with a stereomicroscope, this technology would enable dexterous interaction between a human and a microscopic environment.

Operation in small-scale, often delicate environments requires stable and precise control of manipulator motion. One of the most significant impediments to effective implementation of precision control in micromanipulators is the presence of hard nonlinearities, in particular backlash and Coulomb friction, in the open loop manipulator mechanics [2,4,7,8,11]. The study of direct-drive robots was borne out of the necessity to implement precision position control of robot manipulation for purposes of mechanical interaction [1]. A direct-drive design significantly reduces the amount of backlash and Coulomb friction in the control plant. The elimination of these hard nonlinearities facilitates effective and accurate position, force, impedance, or admittance control of a robot manipulator.

Due to the physics of scaling, devices that operate on a microscopic scale are influenced by highly nonlinear surface forces to a much greater degree than those of a conventional scale [3,12]. Conventional-scale manipulator behavior is typically dominated by inertial effects, which are fundamentally smooth and tend to filter the effects of hard nonlinearities on manipulator motion. The significance of inertial mechanics, however, diminishes with decreasing scale. The magnitude of inertial forces is typically in proportion to volume (assuming invariance of density), and thus scales with the cube of the geometric scaling ratio. As friction is a surface force, the magnitude scales conservatively in proportion to surface area, and thus scales with the square of the geometric scaling ratio. Geometrically similar but smaller devices therefore exhibit increased surface effects and decreased inertial effects, thus exacerbating the control problems presented by non-smooth nonlinearities. If Coulomb friction is independent of surface area, as the conventional conception suggests, then the increased ratio of friction to inertial effects at decreasing scales is even greater.

2 Compliant Mechanism Design

The adverse effects of hard nonlinearities on the performance of robot manipulation (and especially micromanipulation) can be avoided by designing compliant mechanism based "smooth" manipulators. A compliant mechanism is a device that moves solely by deformation, typically by utilizing flexures in place of conventional bearings. Since these devices do not entail any sliding or rolling, they are free of backlash and Coulomb friction, and thus have perfectly smooth mechanics. The absence of hard nonlinearities in compliant mechanism behavior places no fundamental physical limitations on the resolution of position or force control. Additionally, the absence of conventional joints and bearing surfaces produces a clean device that is free of lubricants or other contaminants, and thus is extremely conducive to clean environments. The manipulator described in this paper is a three degree-of-freedom flexure-based position-controlled microrobot.

0-7803-5180-0-5/99 $10.00 © 1999 IEEE

Figure 1 shows a picture of the manipulator which incorporates a five-bar linkage, semi-parallel revolute configuration. The micromanipulator is actuated by flexure suspended voice coils. Instead of a conventional flexure design, the links of the micromanipulator are connected with split-tube flexures. The split-tube flexure, depicted in Figure 2, exhibits a considerably larger range of motion and significantly better multi-axis revolute joint characteristics than a conventional flexure. The design of the joint is based upon contrasting the torsional compliance of an open section with its stiffness in compression and bending. Other references provide an in-depth discussion of the design of the split-tube flexure and micromanipulator [5,6].

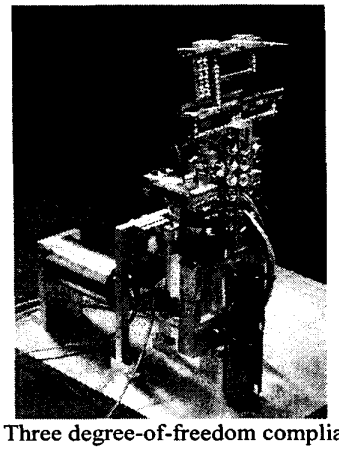

Figure 1. Three degree-of-freedom compliant mechanism-based micromanipulator

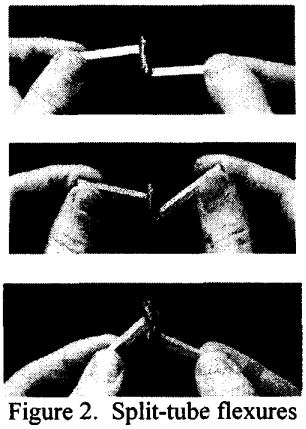

Figure 2. Split-tube flexures

3 Dynamic Equations of the Manipulator

The dynamic behavior of the micromanipulator is different from a conventional manipulator. Specifically, the joints and actuators have stiffnesses, so that the behavior resembles a structure as much as a manipulator. Figure 3 depicts the generalized coordinates of the micromanipulator. The equations of motion for the three degree-of-freedom micromanipulator were obtained using a Lagrangian approach.

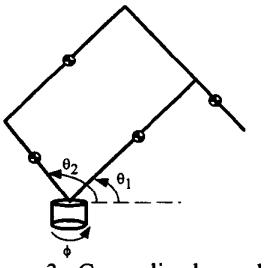

Figure 3. Generalized coordinates

The energies associated with each link of the micromanipulator were defined for a set of rigid links attached by torsional springs. The torsional springs represent the stiffnesses resulting from the split-tube flexures at each joint. Due to the parallel configuration of the manipulator, both the mass and stiffness matrices associated with θ_1 and θ_2 are full, and thus these degrees-of-freedom are highly coupled. The dynamics of the third degree-of-freedom, ϕ, are additionally coupled to the other degrees of freedom.

Before the final dynamic equations can be found, some preliminary relationships must be established. Figures 4, 5, and 6 define the geometric parameters necessary in obtaining the manipulator dynamics. The linear nature of the position and force produced by the voice coils necessitate relationships between the force from each actuator and the corresponding torque on each respective joint. The force-to-torque portion of the compliant mechanism can be modeled by the following set of equations:

$$\tau_{\theta_1} = (u_{\theta_1} - m_{\theta 1}(g + \ddot{x}_{\theta_1}) - b_{\theta 1}\dot{x}_{\theta_1} - k_{\theta 1}x_{\theta_1})A_1 \sin(\mu_{\theta_1}) \quad (1)$$

$$\tau_{\theta_2} = (u_{\theta_2} - m_{\theta 2}(g + \ddot{x}_{\theta_2}) - b_{\theta 2}\dot{x}_{\theta_2} - k_{\theta 2}x_{\theta_2})A_2 \sin(\mu_{\theta_2}) \quad (2)$$

$$\tau_{\phi} = (u_{\phi} - m_{\phi}\ddot{x}_{\phi} - b_{\phi}\dot{x}_{\phi} - k_{\phi}x_{\phi})A_{\phi} \sin(\mu_{\phi}) \quad (3)$$

where $u_{\theta 1}$, $u_{\theta 2}$, and u_{ϕ} are the forces (control inputs) produced by each voice coil; $m_{\theta 1}$, $m_{\theta 2}$, and m_{ϕ} are the masses of the components between the voice coils and their respective links; $b_{\theta 1}$, $b_{\theta 2}$, and b_{ϕ} are the damping constants for each axis of motion; $k_{\theta 1}$, $k_{\theta 2}$, and k_{ϕ} are the spring constants for the parallel flexures which support the voice coil assemblies; A_1, A_2, and A_{ϕ} are constant lengths as defined in Figures 4, 5, and 6; $x_{\theta 1}$, $x_{\theta 2}$, and x_{ϕ} are the displacements of the voice coils; and μ_1, μ_2, and μ_{ϕ} are geometric parameters which are functions of θ_1, θ_2, and ϕ respectively, as defined in Figures 4, 5, and 6. The force inputs (u_i) are additionally saturated at their respective maximum continuous forces. The inverse kinematic relationships between the angular positions of each link and the linear positions of their respective actuators are given by:

$$x_{\theta 1} = A_1 \cos \mu_{\theta_1} + B_1 \cos \alpha_{\theta_1} - D_{01} \quad (4)$$

$$x_{\theta 2} = A_2 \cos \mu_{\theta_2} + B_2 \cos \alpha_{\theta_2} - D_{02} \quad (5)$$

$$x_{\phi} = A_{\phi} \cos \mu_{\phi} + B_{\phi} \cos \alpha_{\phi} - D_{0\phi} \quad (6)$$

where A_1, A_2, A_{ϕ} B_1, B_2, B_{ϕ}, D_{01}, D_{02}, and $D_{0\phi}$ are geometric constants as defined in Figures 4, 5, and 6; $\mu_q = f(q)$ and $\alpha_q = f(q)$. Incorporating the Lagrangian method pre-

viously described, the following equations of motion are obtained for the three degree-of-freedom microrobot.

$$\ddot{\theta}_1 = \frac{1}{H_{11} - \frac{1}{H_{22}} h^2 \cos^2(\theta_1 - \theta_2)} [\frac{-h\cos(\theta_1 - \theta_2)}{H_{22}} (h\dot{\theta}_1^2 \sin(\theta_1 - \theta_2) -$$
$$G_2 \cos\theta_2 - (h\cos\theta_1 \sin\theta_2 + \frac{Q_{21}}{2}\sin 2\theta_2 + Q_{22}(\cos^2\theta_2 - \sin^2\theta_2))\dot{\phi}^2$$
$$- k_{21}(\theta_1 + \theta_{1o}) - k_{22}\theta_2 + k_{21}\theta_{2o} + \tau_{\theta_2}] - h\dot{\theta}_2^2 \sin(\theta_1 - \theta_2) - G_1 \cos\theta_1 \quad (7)$$
$$-(h\sin\theta_1 \cos\theta_2 + \frac{Q_{11}}{2}\sin 2\theta_1 + Q_{12}(\cos^2\theta_1 - \sin^2\theta_1))\dot{\phi}^2$$
$$- k_{11}\theta_1 + k_{11}\theta_{1o} - k_{12}(\theta_2 - \theta_{1o}) + \tau_{\theta_1}$$

$$\ddot{\theta}_2 = \frac{1}{H_{22} - \frac{1}{H_{11}} h^2 \cos^2(\theta_1 - \theta_2)} [\frac{-h\cos(\theta_1 - \theta_2)}{H_{11}} (h\dot{\theta}_2^2 \sin(\theta_1 - \theta_2)$$
$$- G_1 \cos\theta_1 - (h\sin\theta_1 \cos\theta_2 + \frac{Q_{11}}{2}\sin 2\theta_1 + Q_{12}(\cos^2\theta_1 - \sin^2\theta_1))\dot{\phi}^2 \quad (8)$$
$$- k_{11}\theta_1 + k_{11}\theta_{1o} - k_{12}(\theta_2 - \theta_{1o}) + \tau_{\theta_1}] - h\dot{\theta}_1^2 \sin(\theta_1 - \theta_2) - G_2 \cos\theta_2$$
$$-(h\cos\theta_1 \sin\theta_2 + \frac{Q_{21}}{2}\sin 2\theta_2 + Q_{22}(\cos^2\theta_2 - \sin^2\theta_2))\dot{\phi}^2$$
$$- k_{21}(\theta_1 + \theta_{1o}) - k_{22}\theta_2 + k_{21}\theta_{2o} + \tau_{\theta_2}]$$

$$\ddot{\phi} = \frac{1}{H_{33}} [(Q_{11}\dot{\theta}_1 \sin 2\theta_1 + Q_{21}\dot{\theta}_2 \sin 2\theta_2 + 2h\dot{\theta}_1 \sin\theta_1 \cos\theta_2 \quad (9)$$
$$+ 2h\dot{\theta}_2 \cos\theta_1 \sin\theta_2)\dot{\phi} - k_{1\phi}\phi + \tau_\phi]$$

The values of the parameters used to define the sixth-order dynamics are given in the appendix. These parameters consist of the masses and inertias of each link, in addition to other information. The combination of equations 1 through 9 relate the angular output positions (θ_1, θ_2, and ϕ) to the forces applied to each link ($u_{\theta 1}$, $u_{\theta 2}$, and u_ϕ) by each respective voice coil. As seen in the equations, the dynamics are nonlinear with motion along each degree-of-freedom coupled to the other degrees of freedom.

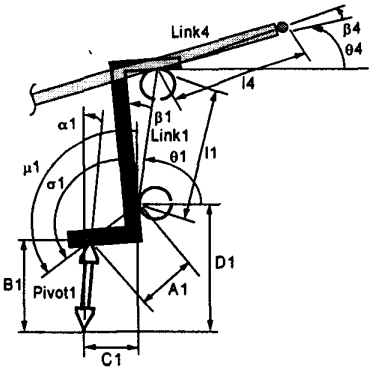

Figure 4. Parameters for θ_1-axis

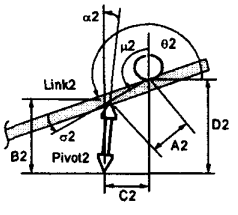

Figure 5. Parameters for θ_2-axis

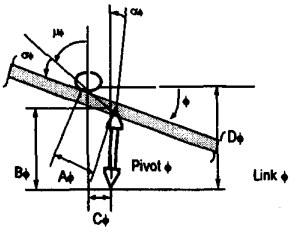

Figure 6. Parameters for ϕ-axis

4 Control of the Micromanipulator

As seen in equations 1 through 9, the model of the manipulator includes several terms that do not typically appear in robot manipulators (i.e., terms involving k_i's). The presence of these terms renders the robot as much a structure as manipulator, resulting in a unique nonlinear control problem. The area of concern with respect to this paper is position control of the micromanipulator. The manipulator was designed to function in a workspace defined by a 2x2x2 cm^3 cube. The objective of the controller is accurate tracking of signals with frequencies approaching 10 to 20 hertz, within the cubic workspace. Control was initially implemented with proportional-derivative control with feedforward stiffness cancellation that resulted in fair but not excellent tracking performance [5,6]. Uncertainties exist in a number of places in the micromanipulator. The parallel flexures used to support the voice coil actuators possess linear stiffness characteristics within certain operating ranges, but behave in nonlinear fashions for large magnitudes of deflection. The constrained motion of the actuators generates slightly curved motion, rather than the assumed rectilinear motion. Other areas of uncertainty include the inertias and masses of the links and other components, and the stiffnesses associated with the split-tube flexures. The significant degree of uncertainty in the manipulator suggests the use of sliding control to achieve robust tracking control. The basis of sliding control lies in replacing the complex control problem with equivalent first-order problems. Following this transformation, the control law maintains tracking stability despite the presence of parametric uncertainty. In its most basic form, a sliding control law incorporates a nominal portion aimed at canceling the nonlinearities, and additional terms that expressly deal with model uncertainty. In principle, optimal performance can be achieved with the transformed (1^{st}-order) problem in the presence of arbitrary parameter errors.

The theory of sliding control provides a systematic approach to stabilization of nonlinear dynamic systems [9]. The control law is defined such that the system trajectory, if not on the sliding surface, s, points towards the surface. The choice of control law is dictated by the following:

$$\frac{1}{2}\frac{d}{dt}s^2 \le -\eta|s| \quad (10)$$

where η is a strictly positive constant that determines the time needed to reach the time-varying sliding surface. The equation above ensures that the distance to the sliding surface, as measured by s^2, always decreases. Because of discontinuity in the control law, overshoot can occur as the system trajectory reaches the sliding surface. This phenomenon leads to chattering in the system trajectory. To alleviate this problem, a boundary layer around the sliding surface is defined to smooth the transition to the sliding surface. The size of the boundary layer is a tradeoff between tracking performance and control activity.

The theory of sliding control can be easily extended to systems with coupled dynamics and multiple inputs, such as robot manipulators [10]. The following equations define the state vector and corresponding sliding surfaces necessary to implement the sliding control law:

$$\underline{x} = [\theta_1, \dot{\theta}_1, \theta_2, \dot{\theta}_2, \phi, \dot{\phi}]^T \tag{11}$$

$$s_{\theta_1} = \dot{\theta}_1 - \dot{\theta}_{1_d} + \lambda_{\theta_1}(\theta_1 - \theta_{1_d}) \tag{12}$$

$$s_{\theta_2} = \dot{\theta}_2 - \dot{\theta}_{2_d} + \lambda_{\theta_2}(\theta_2 - \theta_{2_d}) \tag{13}$$

$$s_{\phi} = \dot{\phi} - \dot{\phi}_d + \lambda_{\phi}(\phi - \phi_d) \tag{14}$$

Once the sliding surface is defined, the control laws for each input ($u_{\theta 1}$, $u_{\theta 2}$, and u_{ϕ}) are determined by the following set of equations:

$$\tau_{\theta_1} = \beta_{11}\dot{\theta}_1^2 + \beta_{12}\dot{\theta}_2^2 + \beta_{13}\dot{\phi}^2 + \beta_{14}\theta_1 + \beta_{15}\theta_2 + \beta_{16} - \varepsilon_1 sat(\frac{s_{\theta_1}}{\Phi_1}) \tag{15}$$
$$+[H_{11} - \tfrac{1}{H_{22}}h^2\cos^2(\theta_1 - \theta_2)] * (\ddot{\theta}_{1_d} - \lambda_{\theta_1}(\dot{\theta}_1 - \dot{\theta}_{1_d}))$$

$$u_{\theta_1} = \frac{-\tau_{\theta_1}}{A_1 \sin \mu_{\theta_1}} + \beta_{17}(g + \ddot{x}_{\theta_1}) + \beta_{18}\dot{x}_{\theta_1} + \beta_{19}x_{\theta_1} \tag{16}$$

$$\tau_{\theta_2} = \beta_{21}\dot{\theta}_1^2 + \beta_{22}\dot{\theta}_2^2 + \beta_{23}\dot{\phi}^2 + \beta_{24}\theta_1 + \beta_{25}\theta_2 + \beta_{26} - \varepsilon_2 sat(\frac{s_{\theta_2}}{\Phi_2}) \tag{17}$$
$$+[H_{22} - \tfrac{1}{H_{11}}h^2\cos^2(\theta_1 - \theta_2)] * (\ddot{\theta}_{2_d} - \lambda_{\theta_2}(\dot{\theta}_2 - \dot{\theta}_{2_d}))$$

$$u_{\theta_2} = \frac{-\tau_{\theta_2}}{A_2 \sin \mu_{\theta_2}} + \beta_{27}(g + \ddot{x}_{\theta_2}) + \beta_{28}\dot{x}_{\theta_2} + \beta_{29}x_{\theta_2} \tag{18}$$

$$\tau_{\phi} = \beta_{31}\dot{\theta}_1\dot{\phi} + \beta_{32}\dot{\theta}_2\dot{\phi} + \beta_{33}\phi - \varepsilon_3 sat(\frac{s_{\phi}}{\Phi_3}) + H_{33}(\ddot{\phi}_d - \lambda_{\phi}(\dot{\phi} - \dot{\phi}_d)) \tag{19}$$

$$u_{\phi} = \frac{-\tau_{\phi}}{A_{\phi} \sin \mu_{\phi}} + \beta_{34}\dot{x}_{\phi} + \beta_{35}x_{\phi} \tag{20}$$

where $\beta_{ij's}$ are the control parameters (given in the appendix) defined to cancel the nonlinear dynamics in each axis of motion; $\lambda_{i's}$ define the dynamics of the system on the sliding surface; $\Phi_{i's}$ define the length of the boundary layer around each sliding surface; $\varepsilon_{i's}$ define the gains on the saturation discontinuities; and the other terms are as previously defined. Provided the uncertainties of the plant are bounded by known values, the $\beta_{ij's}$ are defined such that the controller always compensates for the largest variation that can occur in each parameter. Larger amounts of uncertainty yield larger discontinuity in the control law across the sliding surface.

5 Simulation

Numerical simulation is used to verify the effectiveness of the sliding controller on the micromanipulator. The numerical parameter values needed to define the micromanipulator plant and the additional parameters needed to define the sliding controller are given in the appendix. The stiffnesses of the flexures (split-tube and parallel flexures) were derived for linear, homogeneous, isotropic, deformation-based mechanics. The inertias and masses of each link were calculated using a solid-body modeling computer package.

The micromanipulator and controller were simulated with two different types of inputs: step inputs of various amplitudes and band-limited pseudo random signals. The responses of each axis of the manipulator to step inputs of different amplitudes are shown in Figure 7.

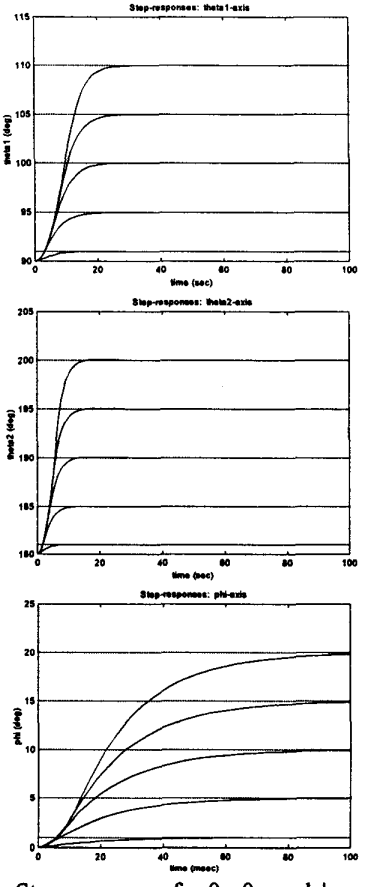

Figure 7. Step-responses for θ_1, θ_2, and ϕ, respectively

To assess the general tracking performance, band-limited pseudo random signals were utilized as command trajectories. The band-limited pseudo random signals are obtained from white noise, which is low-pass filtered and amplitude normalized so as to be within the limits of the micromanipulator. The low-pass filter was implemented with a Fourier transformation, which was used to transform the time-domain white-noise signal to the frequency domain. Once in the frequency domain, the frequencies above the cutoff are removed, and the signal transformed back to the time-domain. The signal was then normalized so that the magnitude was within the manipulator's workspace. The responses of each axis of motion of the microbot to a band-limited pseudo random signal

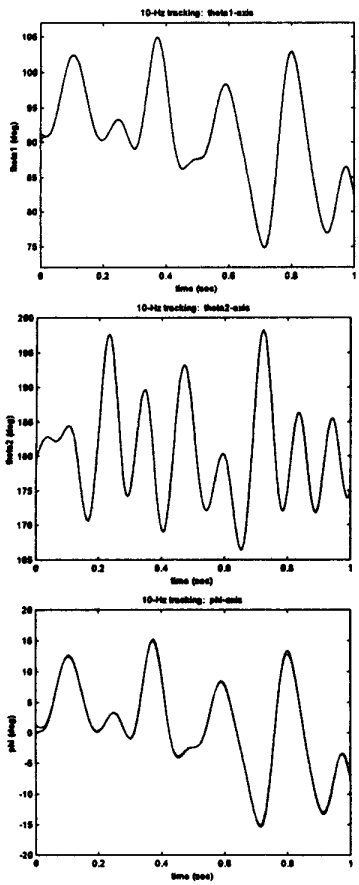

Figure 8. 10-Hz tracking input(--) and output for θ_1, θ_2, and ϕ, respectively

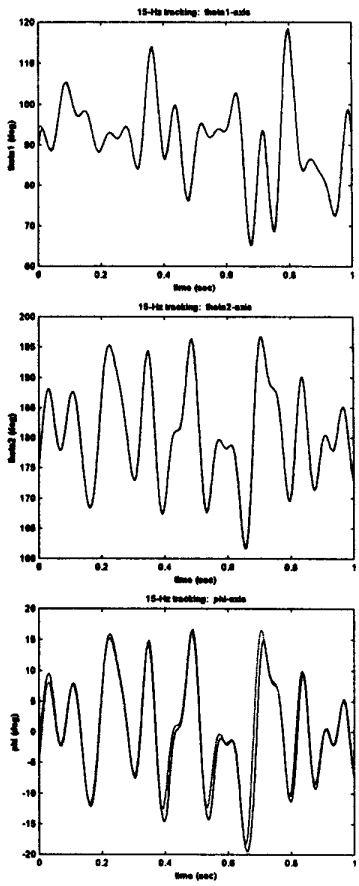

Figure 9. 15-Hz tracking input (--) and output for θ_1, θ_2, and ϕ, respectively

including frequencies up to 10 Hz are shown in Figure 8. The mi cromanipulator with sliding controller tracks the 10-Hz signal with almost no error. The slightest error occurs at the peaks of the desired signal. The responses of each degree of freedom to a 15-Hz pseudo random input are shown in Figure 9. While the tracking degrades somewhat towards the upper and lower limits of the operating range, the manipulator still tracks the desired 15-Hz signal with relatively little error. The 15-Hz pseudo random input approaches the limits of good tracking with the sliding controller, but the bandwidth of the system lies well within the frequency range for which the manipulator was designed.

6 Conclusions

The work in this paper sought to verify the tracking performance of the micromanipulator with a sliding controller. The simulations show that the system achieves the desired bandwidth of operation. Future work with the manipulator will involve experimental validation of the simulated results with the actual manipulator. A sliding controller will be used in testing the micromanipulator with inputs similar to those utilized in simulation. Further development of the uncertainty compensation will be done as is required in attaining the desired performance.

Acknowledgements

Support for this work was provided by NASA Grant No. NGT-8-52839. The authors gratefully acknowledge this support.

References

[1] H. Asada and K. Youcef-Toumi, *Direct-Drive Robots: Theory and Practice*: Cambridge, Massachusetts, MIT Press (1987).

[2] N.G. Chalhoub and A.G. Ulsoy, "Effect of a self-locking drive mechanism on the performance of a flexible robot arm," *Proceedings of the American Control Conference*, pp. 1270-1271 (1990).

[3] R. Fearing, "Survey of Sticking Effects for Micro Parts Handling," *Proceedings of the IEEE/RSJ Conference on Intelligent Robots and Systems*, Vol. 2, pp. 212-217 (1995).

[4] Gogoussis and M. Donath, "Determining the effects of Coulomb friction on the dynamics of bearings and transmissions in robot mechanisms," *ASME Journal of Mechanical Design*, vol. 115, num. 2, pp. 231-240 (1993).

[5] M. Goldfarb and J.E. Speich, "Design of a Minimum Surface-Effect Three Degree-of-Freedom Micromanipulator," *Proceedings of the IEEE Conference on Robotics and Automation*, pp. 1466-1471 (1997).

[6] M. Goldfarb and J.E. Speich, "Eliminating Non-Smooth Nonlinearities with Compliant Manipulator Design,"

Proceedings of the American Controls Conference, pp. 2118-2122 (1998).

[7] E.S. Nakagawa, Y. Uetake, and Z. Cai, "Vibration analysis of robot manipulators: the effect of backlash in transmission mechanisms," *Transactions of the Japan Society of Mechanical Engineers*, vol. 57 no. 544, pp. 3877-3881 (1991).

[8] H. Schempt and D.R. Yoerger, "Study of dominant performance characteristics in robot transmissions," *ASME Journal of Mechanical Design*, vol. 115 num. 3, pp. 472-482 (1993).

[9] J.J. Slotine and W. Li, *Applied Nonlinear Control*: Englewood Cliffs, New Jersy, Prentice Hall (1991).

[10] J.J. Slotine and S.S. Sastry, "Tracking control of nonlinear systems using sliding surfaces, with application to robot manipulators," *International Journal of Control*, pp.465-492 (1983).

[11] W.T. Townsend and J.K. Salisbury, "The effect of Coulomb friction and stiction on force control," *Proceedings of the IEEE Conference on Robotics and Automation*, pp. 883-889 (April 1987).

[12] W. Trimmer and R. Jebens "Actuators for micro robots," *Proceedings of the IEEE International Conference on Robotics and Automation*, pp. 1547-1552 (1989).

Appendix

Relationships for Manipulator Dynamics:

$$h = m_3 g_3 l_2 - m_4 g_4 l_1$$

$$H_{11} = I_{z1} + I_{z3} + m_1 g_1^2 + m_3 g_3^2 + m_4 l_1^2$$

$$H_{22} = I_{z2} + I_{z4} + m_2 g_2^2 + m_3 l_2^2 + m_4 g_4^2$$

$$I_{mg} = (I_{x1} + I_{x3})\sin^2\theta_1 + (I_{x2} + I_{x4})\sin^2\theta_2 + (I_{y1} + I_{y3})\cos^2\theta_1$$

$$+ (I_{y2} + I_{y4})\cos^2\theta_2 - 2Q_{12}\sin\theta_1\cos\theta_2 - 2Q_{22}\sin\theta_2\cos\theta_1\theta_2$$

$$H_{33} = I_\phi + m_1 g_1^2 \cos^2\theta_1 + m_2 g_2^2 \cos^2\theta_2 + m_3 (l_2\cos\theta_2 + g_3\cos\theta_1)^2$$

$$+ m_4 (l_1\cos\theta_1 - g_4\cos\theta_2)^2 + I_{mg}$$

$$G_1 = (m_1 g_1 + m_3 g_3 + m_4 l_1) g$$

$$G_2 = (m_2 g_2 + m_3 l_2 - m_4 g_4) g$$

$$Q_{11} = I_{y1} + I_{y3} - I_{x1} - I_{x3} + m_1 g_1^2 + m_3 g_3^2 + m_4 l_1^2$$

$$Q_{12} = I_{x1y1} + I_{x3y3}$$

$$Q_{21} = I_{y2} + I_{y4} - I_{x2} - I_{x4} + m_2 g_2^2 + m_3 l_2^2 + m_4 g_4^2$$

$$Q_{12} = I_{x2y2} + I_{x4y4}$$

$$k_{11} = k_{1t1} + k_{1t2} + k_{2t2} + k_{3t1} + k_{3t2} + k_{4t1} + k_{4t2}$$

$$k_{112} = k_{1t1} - k_{11}$$

$$k_{21} = -(k_{1t2} + k_{2t2} + k_{3t1} + k_{3t2} + k_{4t1} + k_{4t2})$$

$$k_{22} = k_{2t1} - k_{21}$$

Controller Parameters:

$$\beta_{11} = \frac{h^2 \sin(\theta_1 - \theta_2)\cos(\theta_1 - \theta_2)}{H_{22}}$$

$$\beta_{12} = h\sin(\theta_1 - \theta_2)$$

$$\beta_{13} = \frac{-h\cos(\theta_1 - \theta_2)}{H_{22}}[h\cos\theta_1\sin\theta_2 + \tfrac{Q_{21}}{2}\sin 2\theta_1 + Q_{22}(\cos^2\theta_2 - \sin^2\theta_2)]$$

$$+ h\sin\theta_1\cos\theta_2 + \tfrac{Q_{11}}{2}\sin 2\theta_1 + Q_{12}(\cos^2\theta_1 - \sin^2\theta_1)$$

$$\beta_{14} = \frac{-h\cos(\theta_1 - \theta_2)}{H_{22}} k_{21} + k_{11}$$

$$\beta_{15} = \frac{-h\cos(\theta_1 - \theta_2)}{H_{22}} k_{22} + k_{12}$$

$$\beta_{16} = \frac{h\cos(\theta_1 - \theta_2)}{H_{22}}[-k_{21}\theta_{1o} + k_{2t1}\theta_{2o} - G_2\cos\theta_2 + \tau_{\theta_2}] + G_1\cos\theta_1 - (k_{1t1} + k_{12})\theta_{1o}$$

$$\beta_{17} = m_{\theta 1}$$

$$\beta_{18} = b_{\theta 1}$$

$$\beta_{19} = k_{\theta 1}$$

$$\beta_{21} = h\sin(\theta_1 - \theta_2)$$

$$\beta_{22} = \frac{h^2 \sin(\theta_1 - \theta_2)\cos(\theta_1 - \theta_2)}{H_{11}}$$

$$\beta_{23} = \frac{-h\cos(\theta_1 - \theta_2)}{H_{11}}[h\sin\theta_1\cos\theta_2 + \tfrac{Q_{21}}{2}\sin 2\theta_1 + Q_{12}(\cos^2\theta_1 - \sin^2\theta_1)]$$

$$+ h\cos\theta_1\sin\theta_2 + \tfrac{Q_{21}}{2}\sin 2\theta_2 + Q_{22}(\cos^2\theta_2 - \sin^2\theta_2)$$

$$\beta_{24} = \frac{-h\cos(\theta_1 - \theta_2)}{H_{11}} k_{11} + k_{21}$$

$$\beta_{25} = \frac{-h\cos(\theta_1 - \theta_2)}{H_{11}} k_{12} + k_{22}$$

$$\beta_{26} = \frac{h\cos(\theta_1 - \theta_2)}{H_{11}}[(k_{1t1} + k_{12})\theta_{1o} - G_1\cos\theta_1 + \tau_{\theta 1}] + k_{21}\theta_{1o} - k_{2t1}\theta_{2o} + G_2\cos\theta_2$$

$$\beta_{17} = m_{\theta 2}$$

$$\beta_{18} = b_{\theta 2}$$

$$\beta_{19} = k_{\theta 2}$$

$$\beta_{31} = -Q_{11}\sin 2\theta_1 - 2h\sin\theta_1\cos\theta_2$$

$$\beta_{32} = -Q_{21}\sin 2\theta_2 - 2h\cos\theta_1\sin\theta_2$$

$$\beta_{33} = k_{t\phi}$$

$$\beta_{34} = b_\phi$$

$$\beta_{35} = k_\phi$$

$$\lambda_{\theta_1} = \lambda_{\theta_2} = \lambda_\phi = 500$$

$$\Phi_1 = \Phi_2 = \Phi_3 = 250$$

$$\varepsilon_1 = \varepsilon_2 = 1$$

$$\varepsilon_3 = 2$$

Parameters values for Micromanipulator Dynamics

I_{x1}	2.58e-6 kg*m^2	m_1	5.04e-3 kg
I_{x2}	1.46e-6 kg*m^2	m_2	3.86e-3 kg
I_{x3}	1.38e-6 kg*m^2	m_3	4.75e-3 kg
I_{x4}	1.15e-6 kg*m^2	m_4	4.3e-4 kg
I_{y1}	1.36e-6 kg*m^2	l_1	4.01e-2 m
I_{y2}	1.65e-6 kg*m^2	l_2	2.50e-2 m
I_{y3}	1.24e-7 kg*m^2	g_1	2.32e-2 m
I_{y4}	2.05e-6 kg*m^2	g_2	1.54e-2 m
I_{z1}	1.28e-7 kg*m^2	g_3	2.40e-2 m
I_{z2}	2.01e-7 kg*m^2	g_4	-5.79e-2 m
I_{z3}	1.37e-6 kg*m^2	k_{1t1}	1.00e-2 Nm/rad
I_{z4}	9.08e-7 kg*m^2	k_{1t2}	5.02e-3 Nm/rad
I_{x1y1}	1.19e-7 kg*m^2	k_{2t1}	1.00e-2 Nm/rad
I_{x2y2}	4.41e-10 kg*m^2	k_{2t2}	5.02e-3 Nm/rad
I_{x3y3}	6.06e-8 kg*m^2	k_{3t1}	5.02e-3 Nm/rad
I_{x4y4}	4.59e-16 kg*m^2	k_{3t2}	5.02e-3 Nm/rad
I_{phi}	1.46e-4 kg*m^2	k_{4t1}	1.00e-2 Nm/rad
m_{theta1}	1.88e-2 kg	k_{4t2}	1.00e-2 Nm/rad
m_{theta2}	1.88e-2 kg	k_{tphi}	3.20e-2 Nm/rad
m_{phi}	3.29e-2 kg	k_{theta1}	417 N/m
b_{theta1}	1.0e-1 Ns/m	k_{theta2}	417 N/m
b_{theta2}	1.0e-1 Ns/m	k_{phi}	151 N/m
b_{phi}	5.0e-1 Ns/m		